PNAS RESEARCH ARTICLE | CHEMISTRY

Electrochemically controlled rectification in symmetric single-molecule junctions

Zixiao Wang[a,1], Julio L. Palma[b], Hui Wang[a], Junzhi Liu[c], Gang Zhou[d], M. R. Ajayakumar[e], Xinliang Feng[e], Wei Wang[a], Jens Ulstrup[f,1], Alexei A. Kornyshev[g,1], Yueqi Li[h,1], and Nongjian Tao[a,i]

Edited by Alexis Bell, University of California, Berkeley, Berkeley, CA; received December 8, 2021; accepted July 29, 2022

Single-molecule electrochemical science has advanced over the past decades and now extends well beyond molecular imaging, to molecular electronics functions such as rectification and amplification. Rectification is conceptually the simplest but has involved mostly challenging chemical synthesis of asymmetric molecular structures or asymmetric materials and geometry of the two enclosing electrodes. Here we propose an experimental and theoretical strategy for building and tuning in situ (in operando) rectification in two symmetric molecular structures in electrochemical environment. The molecules were designed to conduct electronically via either their lowest unoccupied molecular orbital (LUMO; electron transfer) or highest occupied molecular orbital (HOMO; "hole transfer"). We used a bipotentiostat to control separately the electrochemical potential of the tip and substrate electrodes of an electrochemical scanning tunneling microscope (EC-STM), which leads to independent energy alignment of the STM tip, the molecule, and the STM substrate. By creating an asymmetric energy alignment, we observed single-molecule rectification of each molecule within a voltage range of ±0.5 V. By varying both the dominating charge transporting LUMO or HOMO energy and the electrolyte concentration, we achieved tuning of the polarity as well as the amplitude of the rectification. We have extended an earlier proposed theory that predicts electrolyte-controlled rectification to rationalize all the observed in situ rectification features and found excellent agreement between theory and experiments. Our study thus offers a way toward building controllable single-molecule rectifying devices without involving asymmetric molecular structures.

tunneling current rectification | symmetric single-molecule junctions | electrolytic control | bipotential control

Significance

Current rectification implies directing an alternating electronic signal into a unified direction and is essential in electronic device functions. Understanding and tuning single-molecule rectification is a core nanoelectronics objective. Previous single-molecule rectification strategies involve mostly asymmetric molecular design or asymmetric enclosing electrode geometry and materials, challenged with chemical synthesis and lack of tunable fine control. We introduce here, experimentally and theoretically, methods and mechanisms for rectification in structurally symmetric single-molecule systems in an electrolyte environment. The rectification ratio was controlled by independently tuning the two electrode potentials and by the ionic strength, while the sign of rectification is determined solely by the electronic structure of the single molecule. Our findings offer a single-molecule phenomenon and identification of single-molecule electron transport mechanisms.

Initially proposed by Aviram and Ratner (1), building a single-molecule electronic rectifier has been an intense focus of theoretical and experimental studies (2–7). The design, synthesis, and physical characterization of such rectifiers are complex tasks, however. The most frequently adopted strategy is to connect an electron donor group with an electron acceptor group (8–12), but the asymmetric molecular design increases the challenges of chemical synthesis and requires additional efforts to organize the molecules in the intended surface orientation. Recent studies have reported rectification in symmetric molecules rooted in highly asymmetric coupling at the two contact interfaces (13–16) and the charge density difference of the two electrodes (17, 18). Accurate, multidimensional control of the rectification ratio in predictable routines remains a challenge, however.

Kornyshev et al. (19) introduced a novel concept and theoretical formalism for the tuning of rectification in symmetric molecular structures in electrolyte junctions. The approach at first rested on molecular superexchange electronic conductivity via a set of lowest unoccupied molecular orbitals (LUMOs), independently controlled by the electrochemical potentials of the tip and substrate electrodes in an electrochemical scanning tunneling microscope (EC-STM). With recognized limitations, the superexchange model can be converted to a direct tunneling form (20). In either mode, rectification originates first from the asymmetric energy barrier height at positive and negative bias created by independent tuning of the tip and substrate electrochemical potentials. Second, the bias voltage variation was shown to depend strongly on the ionic strength in the electrochemically controlled tunneling gap to reinforce the rectification more strongly the higher the ionic strength or shorter the Debye or Gouy screening lengths (19, 20).

In the present work we first report experimental data for single-molecule rectification of two structurally symmetric molecules in electrochemical junctions. We used bipotentially controlled in situ STM to independently tune the tip and substrate energy levels and record single-molecule tunneling current/bias voltage spectroscopy at a fixed electrochemical potential of the STM tip relative to a common reference electrode

The authors declare no competing interest.

This article is a PNAS Direct Submission.

[1]To whom correspondence may be addressed. Email: zixiaowang@smail.nju.edu.cn or ju@kemi.dut.dk or a.kornyshev@imperial.ac.uk or yueqili@ustc.edu.cn.

This article contains supporting information online at http://www.pnas.org/lookup/suppl/doi:10.1073/pnas.2122183119/-/DCSupplemental.

Published September 22, 2022.

(Fig. 1*A*). We have further designed and characterized in both experimental and computational detail two symmetric single-molecule in situ STM rectification probes to investigate the rectification features and mechanism. One probe is an iodo-terminated hexathiophene molecule (IT-6), the other one a circumanthracene-based dibenzonitrile molecule (CABD) (Fig. 1; systematic names, synthesis, and bulk characterization details in *SI Appendix*, Figs. S1–S4). CABD conductivity operates via LUMOs (electron transfer), as addressed in our previous theoretical frames (19, 20), whereas IT-6 operates via a set of highest occupied molecular orbitals (HOMOs; hole transfer). The large conjugated structures of CABD and IT-6 offer small bandgaps so that significant changes in tunneling current can be induced by moderate variation of the electrodes' energy levels. In addition, the large structures offer other fine-tuning options by chemical substitution. Notably, the observed rectification has opposite polarity for CABD (LUMO) and IT-6 (HOMO). Also, as predicted by our model, the experimentally recorded rectification is stronger the higher the ionic strength [see Ref. (19, 20) and the analysis in this paper]. To rationalize these observations in depth we have expanded our previous theoretical frames to accommodate both LUMO and HOMO conducting mechanisms. Having related the theoretical frames with the target molecules, we were able to reproduce the observed differences between the rectification curves for these two kinds of charge transport mechanisms and obtained good agreement with the experimental data. Our work points to an intriguing single-molecule rectification mechanism, ways toward tunable single-molecule rectifying devices, and a method for discerning the mechanisms of electronic charge transfer through single molecules.

Results

The Polarity of Rectification Depends on the Dominating Charge Transport Orbitals. We studied two structurally symmetric molecules, IT-6 (Fig. 1*B*) and CABD (Fig. 1*C*), as structures dominated by HOMO (32) and LUMO (21, 22) electronic charge transport, respectively. The terminal groups of these molecules proved to bind well with Au electrodes (23–26). The molecules were bridged between the substrate and tip Au electrodes of an STM, to be investigated via an electrochemical STM break junction (STM-BJ)technique (Fig. 1*A*) (see *Materials and Methods* for details) (27–30). The Galvani potentials of the tip (φ_t) and working, substrate electrode (φ_s) were controlled independently by the voltage between the tip and reference electrode (V_g) and between the tip and substrate ($V_{bias} = \varphi_s - \varphi_t$) with a bipotentiostat. With φ_t fixed, we varied φ_s in both static and dynamic modes and studied the effect on single-molecule electronic charge transport. The electrochemical potential (V_{EC}) acting on the molecule is taken as the average of φ_t and φ_s. In bipotentiostatically controlled current–voltage (I-V) characteristics, we observed in situ rectification with different directions and curvature for IT-6 (HOMO) and CABD (LUMO) and recorded the dependence of the rectification on the Debye screening length by varying the electrolyte concentration.

In situ rectification of structurally symmetric molecules in electrolyte solution has been described and predicted in theoretical studies (19, 20, 31). A simplified energy diagram (Fig. 2) illustrates the electrochemical rectification mechanism for both HOMO and LUMO charge transport. When we fix the Galvani potential of the tip (φ_t) and vary the Galvani potential of the substrate (φ_s), the tunneling barrier adjacent to the substrate is changed, leading to asymmetric barrier shape and asymmetric overall potential height at positive and negative V_{bias}. The overall potential height of the tunneling barrier for HOMO charge transport increases at negative V_{bias} and decreases at positive V_{bias}.

An opposite V_{bias} dependence is expected for LUMO charge transport, as the negative barrier for hole transport is here replaced by a positive barrier for electron transport. The asymmetric change in the barrier versus V_{bias} affects significantly the tunneling current at different bias polarity, thus leading to electronic rectification. The polarity of V_g determines the barrier shape (bent up or down) in both HOMO and LUMO charge transport but does not affect the mechanism of rectification. The Debye length defines the thickness of the double-layer screening, which is critical for independent control of the tip and substrate potentials and thus for the onset of the rectification.

As noted, previous studies show that charge transport between Au electrodes through IT-6 (32) and nanographene based structures (33) with cyano-terminated groups (23, 34) are dominated by HOMO and LUMO, respectively. To characterize these patterns in detail, we undertook STM-BJ conductance studies with φ_t fixed and φ_s set at different static values (35) (controlled vs. a Ag quasireference electrode in NaF aqueous solution, with potential drift and applicable electrode potentials (36) calibrated; see *SI Appendix*, Fig. S5). NaF aqueous solution was chosen as electrolyte, in which the concentration (i.e., the Debye length) can be precisely controlled, and interference from anion adsorption can be disregarded.

As shown in Fig. 3*A*, the single-molecule conductance of IT-6 in 800 mM NaF aqueous solution is 7.59×10^{-5} G_0 at φ_t = –0.1 V, φ_s = –0.6 V (black, V_{bias} = –0.5 V), and 2.29×10^{-4} G_0 at φ_t = –0.1 V, φ_s = +0.4 V (red, V_{bias} = +0.5 V), where $G_0 = 2e^2/h = 7.768 \times 10^{-5}$ S is the conductance quantum.

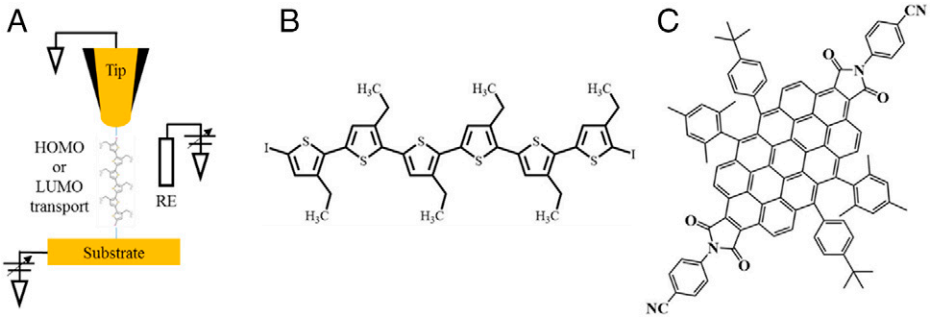

Fig. 1. Scheme of the experimental setup and molecular structures of the bridge molecular species investigated. (*A*) A sketch showing the molecule IT-6 bridged between the coated STM Au tip and Au substrate for studying the asymmetric current response to the bias voltage. The experiments were performed for different concentrations of NaF aqueous solution, with a quasireference Ag electrode (RE) and a Pt counter electrode. (*B*) Molecular structure of IT-6. (*C*) Molecular structure of CABD.

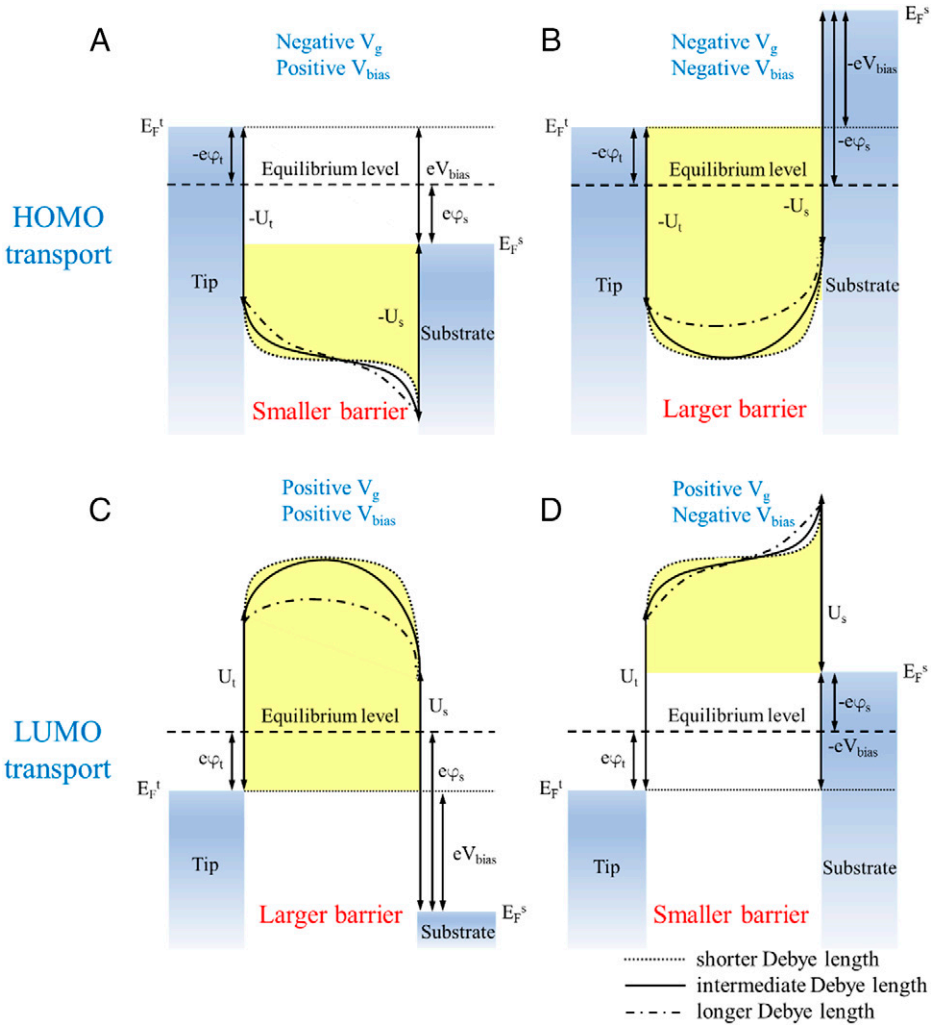

Fig. 2. Energy diagram for independent control of the electrode Galvani potentials in HOMO- and LUMO-dominated charge transport at different ionic strengths: The physical principle of gated current. In the HOMO system at negative V_g, (*A*) positive V_{bias} leads to a smaller barrier, whereas (*B*) negative V_{bias} results in a larger barrier. In the LUMO system at positive V_g, positive V_{bias} leads to a larger barrier (*C*), whereas negative V_{bias} results in a smaller barrier (*D*). The dotted, solid, and dashed-dotted lines represent potential distribution in the solution gap with shorter, intermediate, and longer Debye length, respectively. The shape highlighted in yellow represents the tunneling barrier for shorter Debye length (high ionic strength case, dotted line). ($V_{bias} = \varphi_s - \varphi_t$).

An approximately threefold conductance *increase* is observed for positive V_{bias} compared to negative V_{bias}, when V_{EC} is changed from –0.35 V to +0.15 V. A higher conductance suggests a smaller energy difference between the tunneling barrier and the Fermi level, supporting HOMO-dominated charge transport in IT-6 (17, 37). In contrast, Fig. 3*B* displays an approximately threefold *decrease* for CABD in 800 mM NaF aqueous solution from 1.17×10^{-2} G_0 to 3.72×10^{-3} G_0 in single- molecule conductance when V_{bias} is changed from –0.5 V (black, φ_t = +0.2 V, φ_s = –0.3 V) to +0.5 V (red, φ_t = +0.2 V, φ_s = +0.7 V), and V_{EC} is changed from –0.05 V to +0.45 V, strongly indicative of LUMO charge transport (17, 37). The higher conductance of CABD in contrast to other cyano-terminated groups (38) can be attributed to the small energy gap (shown by ultraviolet–visible [UV–Vis] spectra), the low distance decay constant (23), and better energy alignment between the bulk structure and the contact part of the junction.

The conspicuous but opposite conductance behavior of the two molecular systems is, first, a strong reflection of in situ rectification. Second, the HOMO-dominated system shows positive rectification, the LUMO-dominated system negative rectification. As a control, the conductance of bare Au in the same electrolyte environment shows no conductance peak from molecular junctions in the detectable current regime (*SI Appendix*, Fig. S6).

Tuning the Rectification Amplitude by Independent Control of the Potentials of the Two Electrodes and the Ionic Strength of the Electrolyte. To analyze the electrolyte-controlled rectification phenomenon in detail, we studied the I-V characteristics of the junction for different NaF electrolyte concentrations. φ_t was fixed and φ_s varied. We investigated the dependence of the I-V characteristics on the electrolyte concentration as reflected in the inverse Debye length κ^{-1} (see *SI Appendix*, Fig. S7). Fig. 4*A* and *SI Appendix*, Fig. S8 show representative individual I-V curves of IT-6 (HOMO) where V_{bias} is scanned over ±0.5 V at 10 Hz. The I-V curves display increasingly strong asymmetry from lower (1 mM) to higher (800 mM) electrolyte concentration. The current amplitude is larger at positive V_{bias} than at negative V_{bias}, pointing to a positive rectification. Two-dimensional (2D) I-V histograms constructed from hundreds of individual I-V curves (Fig. 4 *B*–*E*) show in greater detail that the positive rectification is more pronounced at higher electrolyte concentrations.

Fig. 4*F* shows the I-V curves averaged by Gaussian fitting and fitting with polynomial functions, normalized to the dimensional current I_0 (19, 20). The averaged I-V curves suggest a similar trend as the individual I-V curves and the 2D I-V histograms. We define a (maximum) rectification ratio as I(+0.5 V)/I(−0.5 V) for IT-6. The rectification ratio increases from 1.06 to 3.63 as the electrolyte

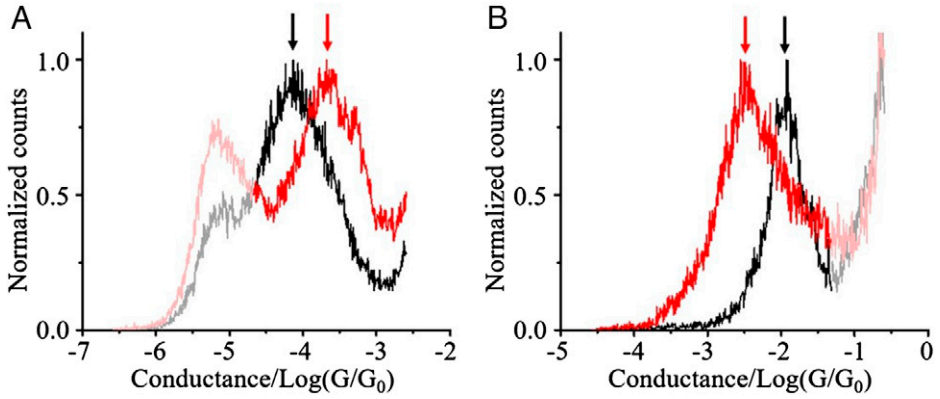

Fig. 3. HOMO and LUMO charge transport across IT-6 and CABD molecular bridges in a gate-controlled STM-BJ. All data refer to 800-mM NaF aqueous electrolyte. (*A*) Conductance histograms of IT-6 (HOMO) recorded at φ_t = –0.1 V, φ_s = –0.6 V (black curve),and φ_t = –0.1 V, φ_s = 0.4 V (red curve). The arrows show that the conductance average is shifted positively as $V_{bias} = \varphi_s - \varphi_t$ increases, indicative of HOMO charge transport. (*B*) Conductance histograms of CABD (LUMO) recorded at φ_t = 0.2 V, φ_s = –0.3 V (black curve) and φ_t = 0.2 V, φ_s = 0.7 V (red curve). The arrows show that the conductance average is here shifted negatively as V_{bias} increases, indicating LUMO charge transport. The low conductance peak in (*A*) and the high conductance feature in (*B*) are from impurities that are insensitive to V_{bias} and V_{EC}.

concentration increases from 1 mM to 800 mM (Table 1). Some of the individual I-V curves display moderate hysteresis, especially at higher currents, which can be attributed to slight molecular conformational changes of the junction at the contact during the V_{bias} sweeping. However, the total trend is not affected as indicated in Fig. 4*F*, where the hysteresis is averaged out.

The molecular length of IT-6, estimated to be 2.5 nm, is longer than the Debye length at 40 mM, 200 mM, and 800 mM, and the longer it is, the stronger the rectification, as expected (19, 20). A higher electrolyte concentration (i.e., shorter Debye length) clearly gives stronger rectification, confirming that electrolyte concentration is a key parameter in precisely tuning the rectification ratio (20). At 1 mM electrolyte concentration, the Debye length is significantly greater than the molecular length, and nearly symmetric I-V curves were observed with rectification ratios around unity.

CABD displays a clearly opposite direction of rectification but, as expected, a similar effect of electrolyte concentration. Individual I-V curves (Fig. 5*A* and *SI Appendix*, Fig. S9), 2D I-V histograms (Fig. 5 *B*–*E*), and averaged normalized I-V curves (Fig. 5*F*) exhibit larger current amplitude at negative V_{bias} compared to positive V_{bias}. We define a (maximum) rectification ratio as I(−0.5 V)/I(+0.5 V) for CABD. The rectification ratio increases from 1.79 to 3.07 when the electrolyte concentration increases from 1 mM to 800 mM. (Table 1 and *SI Appendix*, Fig. S10).

Again, the absolute value of the ratio is larger the higher electrolyte concentration (i.e., the shorter the Debye screening length). The negative rectification ratios for CABD accord with theoretical expectations (20) that negative V_{bias} lowers the barrier and increases the tunneling current for LUMO-dominated charge transport in a bipotentiostatically controlled system. The rectification ratio for both IT-6 and CABD increases approximately linearly with V_{bias} (*SI Appendix*, Fig. S11), offering fine tuning of the single-molecule rectification.

The conductance values extracted from the I-V curves of IT-6 and CABD lead again to the same conclusion that the rectification direction is opposite for the two molecular systems and that rectification is more prominent the higher the electrolyte concentration (*SI Appendix*, Figs. S12 and S13). We note that the slope of the I-V curves (in Fig. 5) and the conductance (*SI Appendix*, Fig. S13) around zero V_{bias} (V_{EC} = –0.2 V) of CABD is lower for higher electrolyte concentrations. This is because LUMO transport dominates CABD charge transport, resulting in lower conductance at negative electrochemical potentials. The conductance change is more pronounced at higher electrolyte concentrations, because the electrochemical potential is more effectively applied on the molecular bridge with a thinner electrochemical double layer.

In situ electrolyte controlled rectification, as observed for IT-6 and CABD, thus appears to be a general phenomenon, but the initial energy difference between the Fermi level and molecular orbital levels is also a key factor in the rectification. From the UV-Vis spectra of IT-6 and CABD (*SI Appendix*, Fig. S2), the bandgaps of IT-6 and CABD are estimated to be 3.01 eV and

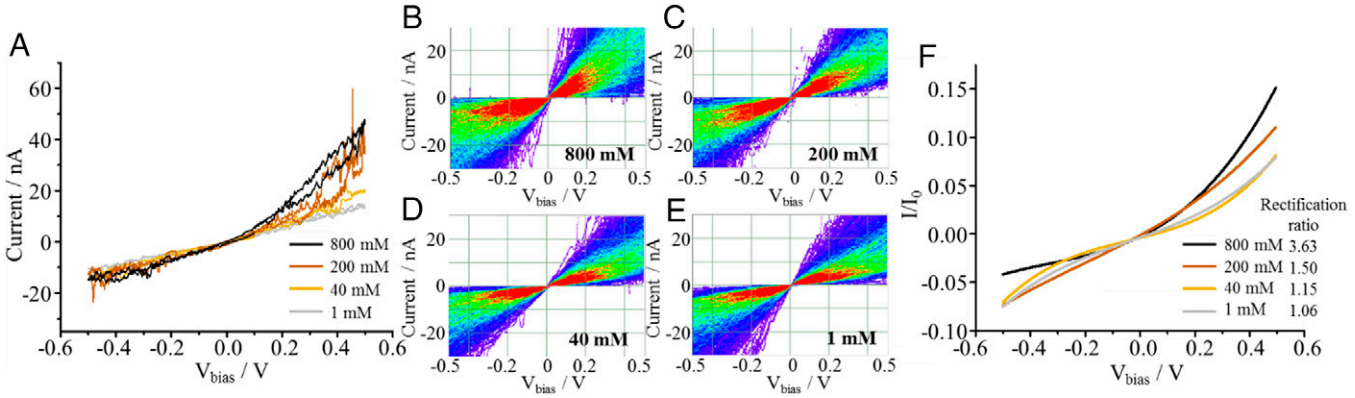

Fig. 4. The effect of electrolyte concentration on I-V characteristics of IT-6. (*A*) Individual I-V curves of IT-6 in different electrolyte concentrations recorded at φ_t = –0.1 V and φ_s = –0.6 V to 0.4 V. (*B*–*E*) I-V 2D histograms of IT-6 at different electrolyte concentrations: (*B*) 800 mM, (*C*) 200 mM, (*D*) 40 mM, and (*E*) 1 mM. (*F*) Normalized fitted I-V curves at the same set of electrolyte concentrations (see main text). The lines are polynomial fittings of the Gaussian maxima at each column bin in *B*–*E* normalized to the dimensional current I_0. The rectification ratios are listed in the figure.

Table 1. Recorded rectification ratios of IT-6 and CABD at ±0.5 V

Electrolyte concentration (mM)	1	40	200	800
Debye length (nm)	9.65	1.53	0.68	0.34
IT-6	1.06	1.15	1.50	3.63
CABD	1.79	2.80	2.63	3.07

1.92 eV, respectively. The relatively narrow bandgaps imply that the energy differences between the Fermi level and the molecular LUMO or HOMO levels are sufficiently small, that measurable changes in tunneling current can be induced by moderate variation of the Fermi level (the electrochemical potentials).

As a control, we recorded the same kind of I-V characteristics for octanedithiol (C8), the LUMO and HOMO levels of which are located far from the Fermi level, and with no overpotential dependence of the tunneling current reported (39). The 2D I-V histograms and averaged I-V curves (*SI Appendix*, Fig. S14) show that the I-V rectification ratio is indeed close to unity (i.e., no rectification) at any electrolyte concentration. The absence of rectification in single-molecule C8 thus demonstrates that the initial energy alignment between the Fermi level and molecular levels is important in the in situ rectification mechanism.

As a further support of the electrolyte-controlled single-molecule rectification mechanism, we undertook another control experiment on CABD (LUMO transport) in a two-electrode system without bipotentiostatic control. In this setup, only the bias voltage between the tip and substrate electrodes, V_{bias}, is defined, while the potentials of the tip and substrate are floating in the V_{bias} scan. As a result, the asymmetric in situ energy alignment no longer stands, and no rectification in the I-V characteristics was observed (*SI Appendix*, Fig. S15). This confirms that the rectification is determined by the independent control of the two electrode potentials in electrochemical junctions.

Altogether these findings strongly support experimentally the concept of electrolytically controlled electrochemical gating of the electronic current for in situ single-molecule rectifiers.

Theoretical and Computational Frames of LUMO and HOMO Single-Molecule Rectification: Calculation of Rectification Curves and Comparison with Experiments. To further rationalize the electrolytic control of single-molecule rectification, we extended our previous theoretical analytical models for superexchange (19) and direct tunneling (20) to include both LUMO and HOMO charge transport.

Electron or hole transfer via a single intermediate LUMO or HOMO state is equivalent to electron or hole tunneling, as represented by the Gamow equation. For LUMO (electron transfer) and HOMO (hole transfer) transport this equation takes the form:

$$\Gamma_{tunn}^{LUMO} = \exp\left\{-\frac{2L}{\hbar}\sqrt{2mU^{LUM}}\right\} \quad [1a]$$

$$\Gamma_{tunn}^{HOMO} = \exp\left\{-\frac{2L}{\hbar}\sqrt{2mU^{HOM}}\right\} \quad [1b]$$

where m is the effective mass of the electron, L the molecular length, and $\hbar$ the Planck's constant; the symbol $U^{\mathrm{LUM}} = (U^{\mathrm{LUMO}} - e_F) > 0$ stands for the LUMO energy relative to the Fermi energy of the electron injecting electrode, e_F, while $U^{\mathrm{HOM}} = (e_F - U^{\mathrm{HOMO}}) > 0$ is the HOMO energy relative to the Fermi energy of the hole injecting electrode. $\mathrm{U}^{\mathrm{LUM}}$ for LUMO (electron) and $\mathrm{U}^{\mathrm{HOM}}$ for HOMO ("hole") conductivity in Eq. 1 are thus both positive. The corresponding superexchange form for electron (LUMO) and hole (HOMO) transport via N identical intermediate states, each of energy U^{LUM} or U^{HOM} and spatial extension between the sites of these states along the molecule, a, would be given by (40)

$$\Gamma_{\mathrm{superexchange}}^{LUMO} = \exp\left\{-\frac{L}{a}\ln\left(\frac{U^{LUM}}{\gamma}\right)\right\} \quad [2a]$$

$$\Gamma_{\mathrm{superexchange}}^{HOMO} = \exp\left\{-\frac{L}{a}\ln\left(\frac{U^{HOM}}{\gamma}\right)\right\} \quad [2b]$$

where γ is the electronic coupling between nearest neighbor intermediate orbitals, the quantity of dimensionality of energy. Eqs. **1** and **2** point to the equivalent exponential distance dependent charge transfer probability of direct tunneling and superexchange. Our analysis in the superexchange framework achieved quantitative accordance with the experimental data. The superexchange form is, however, limited by the condition $|U^{LUM}/\gamma| >> 1$ or $|U^{HOM}/\gamma| >> 1$, which may not apply for CABD and IT-6 (40). It is also difficult to determine the precise number of intermediate states in the two molecular systems. We therefore instead based our data analysis on the simple direct tunneling form.

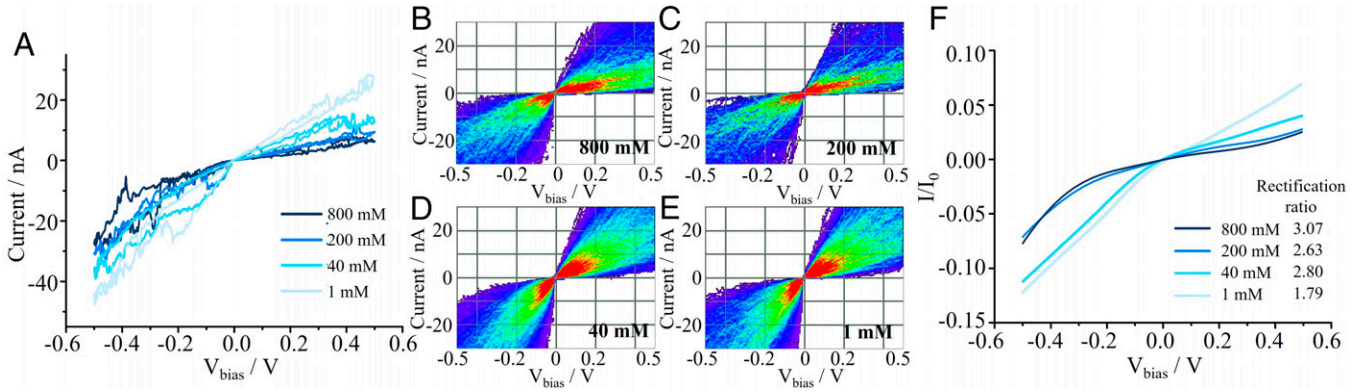

Fig. 5. The effect of electrolyte concentration on I-V characteristics of CABD. (*A*) Individual I-V curves of CABD in different electrolyte concentrations recorded at φ_t = 0.2 V and φ_s = –0.3 V to 0.7 V. (*B*–*E*) I-V 2D histograms of CABD at different electrolyte concentrations: (*B*) 800 mM, (*C*) 200 mM, (*D*) 40 mM, and (*E*) 1 mM. (*F*) Normalized fitted I-V curves at the same set of electrolyte concentrations. The lines are polynomial fittings of the Gaussian maxima at each column bin in *B*–*E* normalized to the dimensional current I_0. The rectification ratios are listed in the figure.

The correlation between the ionic strength–dependent tunneling current through LUMO electron or HOMO hole transport on the bias voltage between the tip and substrate, V_{bias}, can then be described by (20, 31)

$$I^{LUMO} = I_0^{LUMO}\sinh\left(\beta_0^{LUMO}L\frac{eV_{bias}}{4U^{LUM}}\right) \exp\left[-\beta_0^{LUMO}L\frac{eV_{bias}}{4U^{LUM}}\left(1-\frac{tanh(\kappa L/2)}{\kappa L/2}\right)\right] \quad [3a]$$

$$I^{HOMO} = -I_0^{HOMO}\sinh\left(-\beta_0^{HOMO}L\frac{eV_{bias}}{4U^{HOM}}\right) \exp\left[\beta_0^{HOMO}L\frac{eV_{bias}}{4U^{HOM}}\left(1-\frac{tanh(\kappa L/2)}{\kappa L/2}\right)\right] \quad [3b]$$

$$\beta_0^{LUMO} = \frac{2\sqrt{2mU^{LUM}}}{\hbar};\ \beta_0^{HOMO} = \frac{2\sqrt{2mU^{HOM}}}{\hbar} \quad [4]$$

where I is the tunneling current and e the electronic charge. The substrate and tip potentials, φ_s and φ_t, respectively, are controlled independently with respect to the reference electrode, and κ^{-1} is the Debye length. I_0^{LUMO} and I_0^{HUMO} hold the bias voltage independent parts of the dimensional current for the LUMO and HOMO transport cases, respectively.

The barrier heights, U^{LUM} and U^{HOM} were taken as half the HOMO/LUMO band gaps estimated from the UV-Vis spectra and supported by DFT-calculated HOMO/LUMO band gaps as well as by UV-Vis spectra calculated by time-dependent density functional theory (*SI Appendix*, Fig. S2). The resulting values of these quantities were 1.51 eV for IT-6 and 0.96 eV for CABD. The molecular length of the optimized structure was thus obtained from firstprinciple DFT calculation (*SI Appendix*, Fig. S16), the barrier height calculated from the HOMO/LUMO gap, and the Debye length estimated from the ionic strength. We could then calculate the I-V curves for the four studied electrolyte concentrations for IT-6 (Fig. 6*A*) and CABD (Fig. 6*B*). We also calculated the rectification ratios as displayed in Table 2. We note that although the positions of the ethyl substituent groups in the IT-6 thiophene units introduce a slight structural asymmetry, this asymmetry in charge transport is negligible as the ethyl groups do not affect the electronic properties or orbital density (Fig. 6*A*). This was confirmed by comparison with the DFT-calculated frontier orbitals of the iodo-terminated hexathiophene molecule without ethyl substituents (*SI Appendix*, Fig. S17).

The theoretically estimated rectification ratios are thus negative for CABD, the LUMO transport system, and positive for IT-6, the HOMO transport system, both displaying the same polarity as the experimental observations. In addition, the model reproduces the correct trend of the rectification magnitude (i.e., the rectification increases with increasing electrolyte concentration). Notably, at the highest ionic strength (800 mM), the model results in the highest rectification ratios of 4.72 for CABD and 4.36 for IT-6. The experimental values are 3.07 for CABD and 3.63 for IT-6, which accord quite well, considering the generic character and analytical simplicity of the model. Slightly smaller observed rectification values are in fact expected, as not all molecules may be oriented ideally normally to the interface, so that screening will be slightly suppressed (it would have disappeared for strongly tilted molecules). Finally, the variation of the conductance at different ionic strength, which is caused by V_g as predicted by the model, is also successfully reproduced by the experimental data for CABD. The crossover effect is less pronounced for IT-6 in both theoretical estimation and experimental data. This can be traced to the smaller V_g for IT-6 than for CABD.

All this suggests that the theoretical model successfully rationalizes the origin of the electrolytically controlled rectification in symmetric single-molecule junctions with LUMO- or HOMO-dominated charge transport mechanisms. Most notably, it explains what stands behind the difference of the curvatures and rectification polarity of the I-V plots for these two transport scenarios.

Discussion

Our experimental data and theoretical frames have pointed to a single-molecule rectification phenomenon and have emerged as a novel type of electrolytically controlled single-molecule rectification mechanism of two structurally symmetric molecules conducting electronically by LUMO and HOMO charge transport, respectively. Particularly, the opposite signs of the curvature of the I-V rectification curve for HOMO and LUMO transport, in full agreement with the theory, can be a basis for identification of the mechanism of electronic charge transfer through the bridging molecules.

The choice of CABD and IT-6 as model target systems was prompted by several observations. First, these molecules (or molecules with very similar structures) are well characterized in other electronic single-molecule contexts (32, 41, 42). As shown by our experimental and computational results, within the overpotential and bias voltage range applied (a considerable fraction of an electron volt), their charge transport mechanism is entirely dominated by LUMO charge transport for CABD and by HOMO charge transport for IT-6 but without transition into hopping transport with neither electrochemical oxidation of IT-6 nor reduction of CABD, or any accompanying electronic multichannel interference effects. Second, the two molecules are also of comparable lengths and both with relatively high conductance. The 0.5-nm difference in molecular length is small compared with the total lengths of the molecules (2.5 nm+). The molecular lengths fall in our tuning range of the Debye length (0.34 to ~9.65 nm) to enable demonstrating the emergence and enhancement of rectification. The energy gap between the HOMO (IT-6) or LUMO (CABD) and the Fermi energy of the enclosing Au electrodes are small enough to be affected by the bias voltage and overpotential variation, so that rectification can be ensured. Furthermore, along with electrode materials with wider potential windows and wider ionic strength ranges such as in ionic liquid solution, the designed large molecules also offer ways of enhancing the rectification effects by fine tuning the LUMO/HOMO energy gap, for example by ring substitution. Such fine tuning could not be achieved with small molecules.

Our study of single-molecule CABD LUMO conductivity is supported qualitatively and even semiquantitatively by theoretical expectations (19, 20, 31). Together the results demonstrate a negative rectification ratio that depends strongly on the electrolyte concentration for the LUMO-dominated charge transport system under asymmetric energy alignment of the structurally symmetric molecular bridge. We have further shown that the single-molecule conductivity operates by HOMO-dominated charge transport for IT-6 and displays the opposite rectification polarity.

We could rationalize the LUMO/HOMO charge transport duality by our extended theory of molecular rectification in electrolyte junctions that includes both LUMO and HOMO transport modes in the electrolytic in situ tunneling gap.

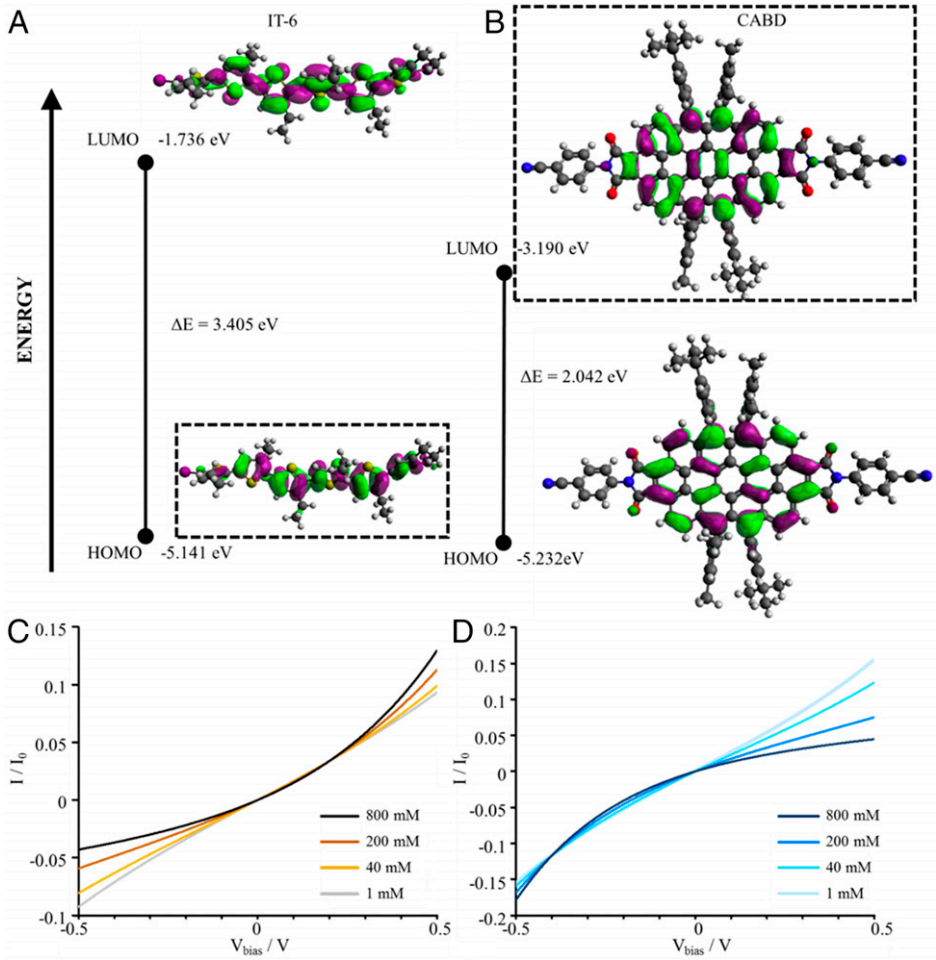

Fig. 6. Calculated results of the energy characteristics of molecular orbitals of the two target bridge molecules, IT-6 (LUMO) (*Left*) and CABD (HOMO) (*Right*) and for the gated rectifications. Frontier molecular orbitals obtained with first-principle calculations based on DFT at the B3LYP/6–-31G(d,p) level and HOMO/LUMO energy gap of (*A*) IT-6 and (*B*) CABD. The single dominating charge transport pathways for IT-6 (HOMO) and CABD (LUMO) are framed by the black dashed boxes. The color code of the molecular structure is H = white, C = gray, N = blue, O = red, and I = purple, while the color code in the isosurfaces represent the negative (green) and positive (purple) phase of the molecular orbitals. Calculations based on the direct tunneling model of electron transport across: (*C*) IT-6 and (*D*) CABD molecular bridges. U^{HOM} is 1.51 eV for IT-6 and U^{LUM} is 0.96 eV for CABD. The rectification ratios for IT-6 are 1.01, 1.43, 2.64, and 4.36 for 1 mM, 40 mM, 200 mM, and 800 mM electrolyte, respectively. The rectification ratios for CABD are 1.01, 1.33, 2.47, and 4.72 for 1 mM, 40 mM, 200 mM, and 800 mM electrolyte, respectively.

Quantitative accordance is limited by the nature of the model used, such as electrolyte Debye-like charge distribution and bulk structural dielectric solvent representations (19, 20). Molecular solvent representations and discrete ionic distributions more sophisticated than the simplest Debye or Gouy views are available (20, 31), however, and can be useful stepping stones for further efforts toward quantitative theoretical and computational accordance with new data.

The extended theory rationalizes the rectification with dual polarity depending crucially on the charge carrier and specific LUMO versus HOMO and is of a magnitude determined by the electrolyte concentration. Comparing the results with experimental data for the chosen two molecules show that a simple model presently is best suited for framing of the data. This choice can be rationalized by the delocalized nature of the electronic LUMO and HOMO states in both IT-6 and CABD that is likely to challenge the ($|U^{LUM}/\gamma| > 1$ or $|U^{HOM}/\gamma| > 1$ condition prerequisite to the superexchange view (19). Strongly delocalized frontier molecular orbitals thus represent lower HOMO–LUMO gaps. This causes a reduction in the energy gap between the dominant molecular orbital (HOMO or LUMO) for the transport mechanism and ε_F and therefore a lowering of the effective tunneling energy barrier (32, 43). In the case of the Gamow model, this would reduce the U^{HOM} and U^{LUM} terms. In no way does it exclude that the superexchange transport mode might be more suitable for other molecules in such nanojunctions, but the sign of the rectification and the qualitative electrolyte effect are the same in the superexchange and direct tunneling models.

Table 2. Calculated rectification ratios of IT-6 and CABD at ±0.5 V

Electrolyte concentration (mM)	1	40	200	800
Debye length (nm)	9.65	1.53	0.68	0.34
IT-6*	1.01	1.43	2.64	4.36
CABD*	1.01	1.33	2.47	4.72

*The calculated molecular length of IT-6 and CABD is 2.54 nm and 3.03 nm.

The IT-6 and CABD molecular probes are attached to the enclosing Au electrodes by iodine and cyanide linking units, respectively. Binding is strong and induces significant electronic delocalization, perhaps even toward Au(0)-I(0)• or Au(0)-NC(0)• radical formation as for Au(0)-thiyl units in thiol self-assembled monolayers (44, 45). In a tunneling view the links would be represented by local fine structure features or "indentations" in the tunneling barrier, quantified by DFT to include the Au-linking

units (44, 45). Such extensions would not affect our observations regarding the electrolytically controlled rectification presently in focus, however.

Previous work reported rectification via asymmetrical energy alignment by environment or gate control. For example, using two-electrode setups, Capozzi et al. (17) demonstrated (in some cases high) rectification of variable-length structurally symmetric oligothiophene-1,1-dioxides (as well as of several other linear symmetric molecules) in polar organic solution, ionic liquid, and aqueous electrolyte. They proposed that rectification is induced by bias voltage–dependent charge density differences between the double layers of the two electrodes, in turn caused by the widely different spatial dimensions of the electrodes. Notably, addition of electrolyte (to propylene carbonate solvent) was concluded not to cause a significant difference from the pure solvent. The rectification ratio was thus concluded to be controlled neither by the electrolyte concentration nor by the independent Galvani potentials of the electrodes. Rectification was also demonstrated by Perrin et al. (46). The energy level difference between the two terminal sites of an asymmetric molecular structure was found to be tuned by both the tip–substrate bias potential and the gate potential. An essential prerequisite of the proposed gate control in their studied particular molecular junction is the asymmetric molecular structure with sophisticated energy level design of each site, however.

In contrast, we have studied rectification in symmetric molecular structures and introduced the asymmetry via fine-tuning of the energy levels of the electrodes and the molecule. In particular, as noted, we have used *independent* Galvani potential control of the tip and the substrate in aqueous NaF solution, itself free of ion adsorption issues. Our focus was furthermore on single molecules in Self-assembled molecular monolayers (SAMs) (instead of in solution, as reported in (17)). Our observations also differ from the notion of charge density caused rectification (17) in that no obvious I-V rectification without independent electrochemical control was observed (*SI Appendix*, Fig. S15). Instead, substantial and ionic strength–dependent rectification was found to appear with independent electrochemical control of the Galvani potentials of the STM tip and the substrate. We have proposed that a possible explanation for the distinct difference between our results and those of reference (17) is that in our SAM layer experiments, nanoprotrusions on the substrate surface created by the break junction process is substantially less covered by molecules and gather charges similarly as the exposed nanoscale area of the coated tip. As a result, when no bipotential control is applied, the charge density is similar at both sides of the single-molecule junction in a SAM layer (see *SI Appendix*, Fig. S18).

The key innovations of our work are therefore:

- Symmetric single-molecule junctions were studied with independent electrochemical potential control of the in situ working electrode and tip, by which single-molecule rectification can be precisely tuned.
- The electrolyte concentration dependence was substantiated experimentally, and with solid theoretical frames, to affect significantly electronic rectification along single-molecule charge transport pathways.
- The physical phenomenon and mechanism disclosed by our work correlate straightforwardly with the rectification direction and amplitude with LUMO or HOMO molecular orbital energy levels, offering wider options of rectification fine tuning by strategic molecular structural design.

Conclusion

In summary, we have explored in detail a mechanism of electrolyte-controlled rectification of two single nonredox molecules in electrolytic in situ STM junctions. The rectification effect for an electrolyte-controlled singlemolecule conductance was predicted 16 years ago, but our present report now presents experimental proof of this effect. Moreover, the extended previous theoretical frames are brought to include electronic charge transport both via a LUMO (electron transport) and a HOMO (hole transport) and to show experimentally and theoretically the dramatic difference between the two cases.

The structurally symmetric large probe molecules were selected, first with a view on their distinct electronic properties, well characterized from comprehensive studies and their small LUMO/HOMO energy gaps, which are paramount for efficient single-molecule electronic function. Such function necessarily requires sophisticated (large, or "smart") molecules. Second, the two probe molecules were selected for their expectedly different—electron (CABD) and hole (IT-6)—transfer mechanisms.

Very notably, the electron (CABD) and hole (IT-6) target molecules were found to display almost exactly opposite rectification behavior (i.e., "negative" rectification for CABD [electron transfer] and "positive" rectification for IT-6 ["hole" transfer]), qualitatively and even semiquantitatively in accordance with the theoretical expectations.

The study demonstrates a general method for tuning the polarity and amplitude of single-molecule rectification by several measures of control that include the dominating charge transport molecular orbitals, the ionic strength, and the bias voltage. We have particularly demonstrated that the electrolyte-controlled rectification needs neither asymmetric molecular structure nor asymmetric electrode contacts, unraveling attractive principles for achieving and tuning rectification. These findings can be expected to stimulate new methods in single-molecule electronics and local solvent environments paving the way for very high ionic concentrations such as ionic liquids.

Materials and Methods

All the synthesis and bulk characterization details are described in *SI Appendix*, Figs. S1–S4.

STM-BJ Measurements. Electrochemically controlled STM-BJ experiments were carried out with an EC-STM (Agilent SPM 5500) consisting of a controller (N9610A, Agilent), and an STM scanner (10 nA/V amplifier, Agilent). The potentials between the STM tip and the substrate (V_{bias}) and between the tip and the reference electrode (V_g) were controlled by DAQ card (National Instruments) and BNC-2110 (National Instruments) through a breakout box (N9227A, Agilent). The STM tip was prepared by cutting a gold wire (0.25 mm diameter, 99.999%, Alfa Aesar) and coated with Apiezon wax to reduce leakage current. A Ag wire and Pt coil were used as quasireference and counter electrode, respectively. The potential drift of the Ag quasireference electrode is shown in *SI Appendix*, Fig. S5*A*. The Au substrate was prepared by magnetron sputtering of Au with a thickness of 47 nm (99.999% purity from Alfa Aesar) on cleaned glass microscope coverslips. Prior to each experiment, the substrate was annealed in a H_2 flame for 1 min to reduce the amount of impurities and then immediately immersed in sample solution overnight for the formation of the SAM. The resulting functionalized substrate was dried in a nitrogen flow. The Teflon liquid cell was cleaned with Piranha (98% H_2SO_4:30% H_2O_2 = 3:1; notes of caution can be found at https://www.drs.illinois.edu/Page/SafetyLibrary/PiranhaSolutions) for 2 h and rinsed with deionized water before each experiment. NaF (99.99%, Alfa Aesar) was used as electrolyte in the electrochemical measurements.

We performed the STM-break-junction measurements via the following two approaches. In the first approach, with fixed potentials between the tip and the

substrate (V_{bias}) and between the tip and the reference electrode (V_g), the tip was repeatedly brought into contact and retracted from the substrate at a constant speed of 21.7 nm/s. Thousands of conductance–distance traces were collected to build the conductance histogram. By measuring the molecular conductance at different, fixed potentials, we obtained the gate effect of IT-6 and CABD from the conductance histograms (Fig. 3 *A* and *B*). In the second approach, single-molecule bipotentiostatically controlled I-V characteristics were recorded for single-molecule junctions. We first carried out single-molecule conductance measurement at fixed potentials. When a plateau indicating the formation of molecular junction was detected, the tip was held in position, and with fixed V_g, V_{bias} was swept within the indicated range at 1 V/s with the tunneling current recorded, from which an I-V curve was obtained. The potential sweeps were recorded from both directions and was repeated thousands of times to construct the 2D I-V histograms (Figs. 4 *B–E* and 5 *B–E*).

DFT Calculations. We performed first-principle DFT calculations of the isolated molecules, IT-6 and CABD, by using the B3LYP density functional and the 6-31G(d,p) basis set (47) as implemented in Gaussian 16 (48). Geometry optimizations followed by vibrational frequency calculations were performed to obtain the minimum energy geometries and the molecular orbital energies. We also performed time-dependent DFT calculations to obtain the theoretical UV–Vis spectrum for both systems considering 20 singlet excited states by using the same density functional and basis set.

Data, Materials, and Software Availability. All study data are included in the article and/or supporting information.

ACKNOWLEDGMENTS. This work was supported by the National Natural Science Foundation of China (grant nos. 21773117, 21904062, and 22174134; CAS Project for Young Scientists in Basic Research). All the authors are grateful to the late Professor Nongjian Tao for his insightful instruction on the key part of the experimental work. J.U., A.A.K., and Y.L. are thankful to K. C. Matthew Cheung for useful discussions of theoretical calculations and to Dr. Ture Damhus for useful discussions and help with the target molecular nomenclature. J.U. and A.A.K. acknowledge the collaboration on this topic in the past with late Professor A. M. Kuznetsov, with whom the first principles of single-molecule rectification in electrolyte solution were formulated.

Author affiliations: [a]State Key Laboratory of Analytical Chemistry for Life Science, School of Chemistry and Chemical Engineering, Nanjing University, Nanjing 210023, China; [b]Department of Chemistry, Pennsylvania State University, Fayette, The Eberly Campus, Lemont Furnace, PA 15456; [c]Department of Chemistry and State Key Laboratory of Synthetic Chemistry, the University of Hong Kong, Hong Kong, China; [d]Laboratory of Advanced Materials, State Key Laboratory of Molecular Engineering of Polymers, Fudan University, Shanghai 200438, China; [e]Centre for Advancing Electronics Dresden, Faculty of Chemistry and Food Chemistry, Technische University Dresden, 01062 Dresden, Germany; [f]Department of Chemistry, Technical University of Denmark, Kongens Lyngby 2800, Denmark; [g]Department of Chemistry, Imperial College London, Molecular Sciences Research Hub, White City Campus, London W12 0BZ, United Kingdom; [h]Center for Bioanalytical Chemistry, University of Science and Technology of China, Hefei 230026, China; and [i]Center for Bioelectronics and Biosensors, Biodesign Institute and School of Electrical, Energy and Computer Engineering, Arizona State University, Tempe, AZ 85287

Author contributions: Z.W., H.W., Y.L., and N.T. designed research; Z.W. and Y.L. performed research; J.L., G.Z., M.R.A., and X.F. contributed new reagents/analytic tools; Z.W., J.L.P., W.W., J.U., A.A.K., and Y.L. extended and adjusted the theory and analyzed data; and Z.W., J.U., A.A.K., and Y.L. wrote the paper.

1. A. Aviram, M. A. Ratner, Molecular rectifiers. *Chem. Phys. Lett.* **29**, 277–283 (1974).
2. A. M. Kuznetsov, J. Ulstrup, Mechanisms of molecular electronic rectification through electronic levels with strong vibrational coupling. *J. Chem. Phys.* **116**, 2149–2165 (2002).
3. I. Díez-Pérez *et al.*, Rectification and stability of a single molecular diode with controlled orientation. *Nat. Chem.* **1**, 635–641 (2009).
4. A. Batra *et al.*, Molecular diodes enabled by quantum interference. *Faraday Discuss.* **174**, 79–89 (2014).
5. S. Fujii *et al.*, Rectifying electron-transport properties through stacks of aromatic molecules inserted into a self-assembled cage. *J. Am. Chem. Soc.* **137**, 5939–5947 (2015).
6. J. Trasobares, D. Vuillaume, D. Théron, N. Clément, A 17 GHz molecular rectifier. *Nat. Commun.* **7**, 12850 (2016).
7. N. Zhang, W.-Y. Lo, Z. Cai, L. Li, L. Yu, Molecular rectification tuned by through-space gating effect. *Nano Lett.* **17**, 308–312 (2017).
8. R. M. Metzger, Unimolecular electrical rectifiers. *Chem. Rev.* **103**, 3803–3834 (2003).
9. A. Batra *et al.*, Tuning rectification in single-molecular diodes. *Nano Lett.* **13**, 6233–6237 (2013).
10. M. Souto *et al.*, Tuning the rectification ratio by changing the electronic nature (open-shell and closed-shell) in donor–acceptor self-assembled monolayers. *J. Am. Chem. Soc.* **139**, 4262–4265 (2017).
11. R. Yamada *et al.*, Single-molecule rectifiers based on voltage-dependent deformation of molecular orbitals in carbazole oligomers. *Nanoscale* **10**, 19818–19824 (2018).
12. M. Baghbanzadeh *et al.*, Dipole-induced rectification across Ag^{TS}/SAM//Ga_2O_3/EGaIn junctions. *J. Am. Chem. Soc.* **141**, 8969–8980 (2019).
13. D. Janes, Molecular electronics: Rectifying current behaviours. *Nat. Chem.* **1**, 601–603 (2009).
14. T. Kim, Z.-F. Liu, C. Lee, J. B. Neaton, L. Venkataraman, Charge transport and rectification in molecular junctions formed with carbon-based electrodes. *Proc. Natl. Acad. Sci. U.S.A.* **111**, 10928–10932 (2014).
15. K. Wang, J. Zhou, J. M. Hamill, B. Xu, Measurement and understanding of single-molecule break junction rectification caused by asymmetric contacts. *J. Chem. Phys.* **141**, 054712 (2014).
16. M. Iwane, S. Fujii, M. Kiguchi, Molecular diode studies based on a highly sensitive molecular measurement technique. *Sensors (Basel)* **17**, 5 (2017).
17. B. Capozzi *et al.*, Single-molecule diodes with high rectification ratios through environmental control. *Nat. Nanotechnol.* **10**, 522–527 (2015).
18. H. Atesci *et al.*, Humidity-controlled rectification switching in ruthenium-complex molecular junctions. *Nat. Nanotechnol.* **13**, 117–121 (2018).
19. A. A. Kornyshev, A. M. Kuznetsov, J. Ulstrup, In situ superexchange electron transfer through a single molecule: A rectifying effect. *Proc. Natl. Acad. Sci. U.S.A.* **103**, 6799–6804 (2006).
20. K. C. M. Cheung, X. Chen, T. Albrecht, A. A. Kornyshev, Principles of a single-molecule rectifier in electrolytic environment. *J. Phys. Chem. C* **120**, 3089–3106 (2016).
21. S. Y. Quek *et al.*, Mechanically controlled binary conductance switching of a single-molecule junction. *Nat. Nanotechnol.* **4**, 230–234 (2009).
22. J. Koga, Y. Tsuji, K. Yoshizawa, Orbital control of single-molecule conductance perturbed by pi-accepting anchor groups: Cyanide and isocyanide. *J. Phys. Chem. C* **116**, 20607–20616 (2012).
23. P. Moreno-García *et al.*, Single-molecule conductance of functionalized oligoynes: Length dependence and junction evolution. *J. Am. Chem. Soc.* **135**, 12228–12240 (2013).
24. D. Z. Manrique, Q. Al-Galiby, W. Hong, C. J. Lambert, A new approach to materials discovery for electronic and thermoelectric properties of single-molecule junctions. *Nano Lett.* **16**, 1308–1316 (2016).
25. L.-L. Peng *et al.*, Low tunneling decay of iodine-terminated alkane single-molecule junctions. *Nanoscale Res. Lett.* **13**, 121 (2018).
26. Y. Li *et al.*, Gate controlling of quantum interference and direct observation of anti-resonances in single molecule charge transport. *Nat. Mater.* **18**, 357–363 (2019).
27. S. Boussaad, N. J. Tao, Atom-size gaps and contacts between electrodes fabricated with a self-terminated electrochemical method. *Appl. Phys. Lett.* **80**, 2398–2400 (2002).
28. B. Xu, N. J. Tao, Measurement of single-molecule resistance by repeated formation of molecular junctions. *Science* **301**, 1221–1223 (2003).
29. Y. Li *et al.*, Transition from stochastic events to deterministic ensemble average in electron transfer reactions revealed by single-molecule conductance measurement. *Proc. Natl. Acad. Sci. U.S.A.* **116**, 3407–3412 (2019).
30. J. Bai *et al.*, Anti-resonance features of destructive quantum interference in single-molecule thiophene junctions achieved by electrochemical gating. *Nat. Mater.* **18**, 364–369 (2019).
31. A. A. Kornyshev, A. M. Kuznetsov, A new type of in situ single-molecule rectifier. *Chem Phys Chem* **7**, 1036–1040 (2006).
32. L. Xiang *et al.*, Non-exponential length dependence of conductance in iodide-terminated oligothiophene single-molecule tunneling junctions. *J. Am. Chem. Soc.* **138**, 679–687 (2016).
33. T. Enoki, M. Kiguchi, Challenges for single molecule electronic devices with nanographene and organic molecules. Do single molecules offer potential as elements of electronic devices in the next generation? *Phys. Scr.* **93**, 5 (2018).
34. L. A. Zotti *et al.*, Revealing the role of anchoring groups in the electrical conduction through single-molecule junctions. *Small* **6**, 1529–1535 (2010).
35. C. Wu *et al.*, A chemically soldered polyoxometalate single-molecule transistor. *Angew. Chem. Int. Ed. Engl.* **59**, 12029–12034 (2020).
36. G. Lovat *et al.*, Room-temperature current blockade in atomically defined single-cluster junctions. *Nat. Nanotechnol.* **12**, 1050–1054 (2017).
37. Y. Zang *et al.*, Resonant transport in single diketopyrrolopyrrole junctions. *J. Am. Chem. Soc.* **140**, 13167–13170 (2018).
38. K. Yoshida *et al.*, Correlation of breaking forces, conductances and geometries of molecular junctions. *Sci. Rep.* **5**, 9002 (2015).
39. H. Wang *et al.*, Potential dependence of mechanical stability and electronic coupling of single S–Au bonds. *J. Am. Chem. Soc.* **140**, 18074–18081 (2018).
40. J. D. Zhang *et al.*, Electrochemistry and bioelectrochemistry towards the single-molecule level: Theoretical notions and systems. *Electrochim. Acta* **50**, 3143–3159 (2005).
41. A. Mishchenko *et al.*, Single-molecule junctions based on nitrile-terminated biphenyls: A promising new anchoring group. *J. Am. Chem. Soc.* **133**, 184–187 (2011).
42. I. Diez-Perez *et al.*, Gate-controlled electron transport in coronenes as a bottom-up approach towards graphene transistors. *Nat. Commun.* **1**, 31 (2010).
43. Y. Zang *et al.*, Cumulene wires display increasing conductance with increasing length. *Nano Lett.* **20**, 8415–8419 (2020).
44. J. R. Reimers, M. J. Ford, A. Halder, J. Ulstrup, N. S. Hush, Gold surfaces and nanoparticles are protected by Au(0)-thiyl species and are destroyed when Au(I)-thiolates form. *Proc. Natl. Acad. Sci. U.S.A.* **113**, E1424–E1433 (2016).
45. J. R. Reimers, M. J. Ford, S. M. Marcuccio, J. Ulstrup, N. S. Hush, Competition of van der Waals and chemical forces on gold-sulfur surfaces and nanoparticles. *Nat. Rev. Chem.* **1**, 0017 (2017).
46. M. L. Perrin *et al.*, A gate-tunable single-molecule diode. *Nanoscale* **8**, 8919–8923 (2016).
47. W. J. Hehre, L. Radom, P. V. R. Schleyer, J. A. Pople, *Ab Initio Molecular Orbital Theory* (John Wiley, New York, 1986).
48. M. J. Frisch *et al.*, *Gaussian 16, Revision A.03* (Gaussian, Inc., Wallingford, CT, 2016).